Functional Microporous Polymer Networks: Synthesis and Applications

Alex Palma-Cando and Ullrich Scherf

Abstract Microporous polymer networks (MPNs) possess a high potential for such applications where high specific surface areas and extended π-conjugation (causing semiconductive properties) are a must. Some relevant experimental results for chemical and electrochemical generation of functional microporous polymer networks gathered during the last decade in our groups are here presented. Smart design of rigid 3D building blocks (tectons) allows to produce microporous polymers with specific surface areas up to 2200 m^2 g^{-1}. Microporous monoliths have been e.g. used for oil trapping from aqueous mixtures while thin MPN films showed a high potential in the optical and electrochemical detection of nitroaromatic explosives up to low ppb concentrations.

Keywords Microporous Polymer Networks (MPNs) · Electrodeposition · Electrochemical sensing · Optical sensing · Nitroaromatic analytes · Thin film sensors · Polymer monoliths

Abbreviations

AFM	Atomic force microscopy
AIE	Aggregation-induced emission
BFEE	Boron trifluoride ethyl etherate
CMP	Conjugated microporous polymer
CPMAS	Cross-polarization magic-angle spinning
DCM	Dichloromethane

A. Palma-Cando
School of Chemical Sciences and Engineering, Materials and Processes Applied Research Group (GIAMP), Yachay Tech University, Hda. San José s/n y Proyecto Yachay, 100119 Urcuquí, Ecuador

U. Scherf (✉)
Macromolecular Chemistry Group and Wuppertal Institute for Smart Materials and Systems, Bergische Universität Wuppertal, Gaußstraße 20, 42119 Wuppertal, Germany
e-mail: scherf@uni-wuppertal.de

M. J. M. Abadie et al. (eds.), *New Trends in Macromolecular and Supramolecular Chemistry for Biological Applications*, https://doi.org/10.1007/978-3-030-57456-7_4

DMI	1,3-Dimethyl-2-imidazolidinone
DNB	1,3-Dinitrobenzene
DNT	2,4-Dinitrotoluene
EQCM	Electrochemical quartz-crystal microbalance
GC	Glassy Carbon
HCP	Hypercrosslinked polymers
ITO	Indium tin oxide
LSV	Linear sweep voltammetry
MPN	Microporous polymer network
NB	Nitrobenzene
ODB	1,2-Dichlorobenzene
PAF	Porous aromatic framework
PL	Photoluminescence
p-$TolSO_2Na$	Sodium p-toluenesulfinate
Rq	Root-mean-square roughness
S_{BET}	Brunauer−Emmett−Teller specific surface areas
$TBABF_4$	Tetrabutylammonium tetrafluoroborate
TBAF	Tetrabutylammonium fluoride
TBAP	Tetrabutylammonium perchlorate
TDAE	Tetrakis(dimethylamino)ethylene
THF	Tetrahydrofurane
TNB	1,3,5-Trinitrobenzene
TNP	2,4,6-Trinitrophenol
TNT	2,4,6-Trinitrotoluene
TPE	Tetraphenylethylene
WE	Working electrode

1 Introduction

Polymerization of bifunctional monomers usually leads to the formation of 1D-linear or branched, non-porous polymers. By chemical modification of a precursor polymer, hypercrosslinked polymers (HCPs) have been produced using different cross-likers (Tan and Tan 2017). These HCPs showed *high Brunauer−Emmett−Teller* (BET)-derived surface areas (S_{BET}) up to 3000 $m^2\ g^{-1}$ (Wang et al. 2017). A different approach for synthesizing porous polymer structures is based on the polymerization of rigid, multifunctional 3D monomers. The resulting, mostly amorphous materials are covalently bond and highly crosslinked organic structures that present inherent microporosity (porous diameter < 2 nm) (Sing et al. 1984) and high surface areas (Preis et al. 2015a). Conjugated microporous polymers (CMPs) (Lee and Cooper 2020) and porous aromatic frameworks (PAFs) (Yuan and Zhu 2019) are common names used to described these type of polymer networks. Only difference between CMPs and PAFs is the occurrence/non-occurrence of extended π-conjugation thus

causing problems in the classification of (micro)porous polymers (Jiang et al. 2007). To avoid misunderstandings, we have opted for a different terminology, Microporous Polymer Networks (MPNs), which includes both CMPs and PAFs. MPNs have shown application potential in gas storage and separation (Lu et al. 2010), adsorption and encapsulation of chemicals (Wang et al. 2013), heterogeneous catalysis (Xie et al. 2013), photoredox catalysis (Zhang et al. 2013), light emittance (Bonillo et al. 2016), chemo- and biosensing (Geng et al. 2016), energy storage (Zhang et al. 2018), and in biological applications (Bhunia et al. 2018). Synthesis chemical routes for the production of MPNs are mainly dealing with C-C coupling or C-N coupling reactions such as Sonogashira-Hagihara coupling (Trunk et al. 2016), Suzuki-Miyaura coupling (Chen et al. 2010), Yamamoto coupling (Schmidt et al. 2009), Heck coupling (Sun et al. 2013), cyclotrimerizations (Buyukcakir et al. 2019), phenazine ring fusion (Marco et al. 2017), Schiff-base condensations (Xu and Hedin 2013), heterocycle linkages (Biswal et al. 2018), alkyne metathesis (Lu et al. 2015), Buchwald-Hartwig amination (Liao et al. 2018), direct arylation (Liu et al. 2013), polyolefinations (Preis et al. 2015a), and oxidative couplings (Qiao et al. 2014). MPNs produced by these chemical routes are usually insoluble and practically intractable powders or monoliths that cannot be processed into thin films for applications in the field of organic electronics. Electrochemical, oxidative generation of MPNs has proved to be an promising technique for the preparation of high quality thin MPN films (Suresh and Scherf 2018). The electropolymerization method allows for simultaneous MPN formation and deposition under mild and catalyst-free conditions, and in short times. Anodic electropolymerization is accomplished by oxidation of multifunctional monomers at the electrode followed by cascades of radical ion-radical ion coupling reactions which leads to dimers, trimers, tetramers, oligomers up to polymer networks (Ibanez et al. 2018). A controlled deposition of the growing thin MPN films on the electrode surface is driven by a progressively reduced solubility of the coupling products (Heinze et al. 2010). Thiophenes and carbazoles are the most used electroactive motifs with low oxidation potential, that are applied in combination with suitable linkers in the electrogeneration of MPN films (Palma-Cando et al. 2019a; Zhang et al. 2015).

Hereinafter, we discuss some of our efforts and contributions in the synthesis, characterization and application of microporous polymer networks during the past decade. A library of diverse monomers utilized for the generation of MPNs is presented in Scheme 1. In the first part, we review some examples of chemically synthesized MPNs based on cyclotrimerizations and Friedel-Craft-type polycondensations. Then, we will focus on the electrochemical generation of thin MPN films based on multifunctional carbazole- and thiophene-based rigid monomers and their application as luminescent or electrochemical sensors for nitroaromatic analytes. Both oxidative chemical or electrochemical polymerizations have been comparatively studied, e.g. concerning the inherent porosity of bulk powders and thin MPN films, respectively.

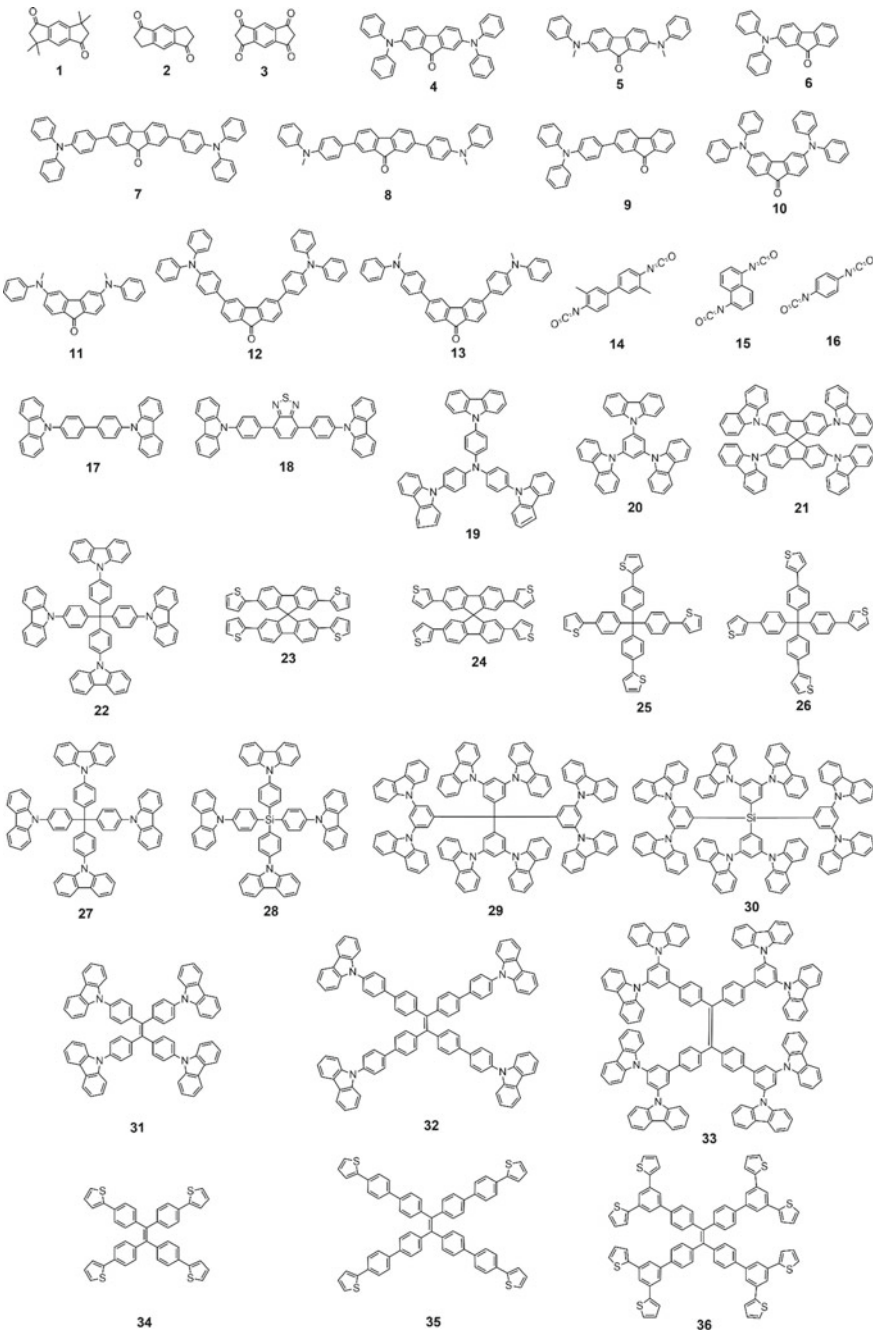

Scheme 1 Chemical structures of chemically or electrochemically polymerized monomers for generation of microporous polymer networks (MPNs)

2 Chemically Synthesized Microporous Polymer Networks

A first selected approach in the synthesis of microporous polymer networks is based on a well-known synthesis of truxene derivatives by cyclotrimerization, here by using bifunctional s-indacene monomers (Sprick et al. 2010). Truxene itself is obtained in the cyclotrimerization of indan-1-one with protic (Dehmlow and Kelle 1997) or Lewis acids (Ansems et al. 2000), while truxenone can be synthesized in the condensation of indan-1,3-dione with protic acids (Sanguinet et al. 2006). Figure 1 shows the chemical structures of our bifunctional monomers **1–3**. Polycondensation of monomer **1** was tested under different acidic conditions resulting in a MPN yield of ca. 85% by using titanium tetrachloride as Lewis acidic catalyst in 1,2-dichlorobenzene (180 °C, 72 h). Monomers **2** and **3** were polymerized under similar conditions using titanium tetrachloride (for 72 h) or methanensulfonic acid (for 3 h), respectively, with a quantitative polymer yield. Idealized structures of the resulting ladder-type MPNs are shown in Fig. 1. These network polymers showed excellent thermal stability in air up to 330 °C. Solid state ^{13}C $\{^{1}H\}$ cross-polarization magic-angle spinning (CPMAS) NMR spectroscopy confirmed the formation of the idealized structural motifs including low-intensity carbonyl-related end group signals. Surface area (S_{BET}) values of the bulk polymers were obtained by applying the Brunauer–Emmett–Teller equation to the corresponding nitrogen adsorption isotherms. **P1** showed a S_{BET} value of 395 m^2 g^{-1} which was much lower than the S_{BET} values of 1165 m^2 g^{-1} for **P2** possibly related to the presence of bulkier methyl substituents that support pore formation. **P3** showed the highest S_{BET} value of 1650 m^2 g^{-1} for a MPN powder obtained in a metal-free, acid catalyzed cyclotrimerization.

As second example of our selection, acid-catalysed Friedel-Craft-type polycondensations were applied to a series of 10 multifunctional arylamino-substituted fluorenone monomers (see monomers **4–13** in Scheme 1) and binary mixtures of them

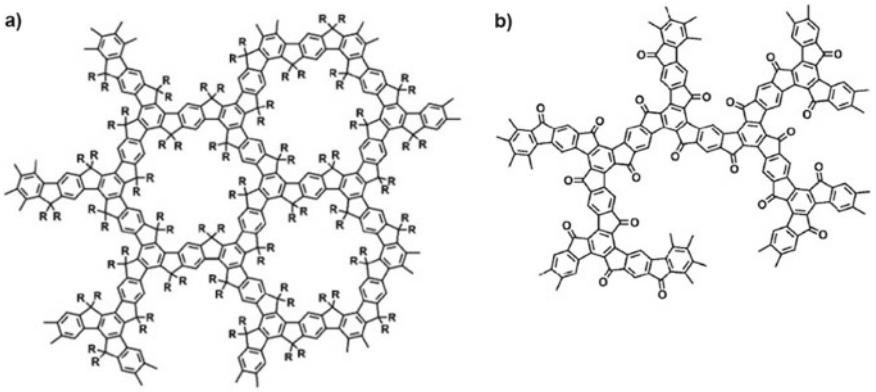

Fig. 1 Idealized chemical structures of MPNs **a** P1 and P2 (P1: R = CH_3, P2: R = H), and **b** P3. (Sprick et al. 2010). Reproduced with permission of The Royal Society of Chemistry

(Preis et al. 2011). $A_2 + B_2$ and AB_2 polycondensations under Friedel-Craft reaction conditions between aromatic ketones and bifunctional aromatic moieties lead to the formation of linear, high molecular weight polymers (Zolotukhin et al. 2004) and hyperbranched polymers, (Smet et al. 2002) respectively. We used the similar synthetic principles for the generation of MPNs (for **P4–P6** see Fig. 2) starting from A_4B_2 and A_2B_2 monomers, carried out with methane sulfonic acid as catalyst in 1,2-dichlorobenzene (at 140 °C). Formation of rigid, three-dimensional (3D) structures was obtained in a single reaction step under formation of 9,9-diphenylfluorene knot motifs in nearly quantitative yields. Thermogravimetric analysis showed good stability of the MPNs up to 250 °C. Solid-state $^{13}C\{^1H\}$ CPMAS NMR spectra for **P4** showed a broad signal with three maxima at 129 ppm, 138 ppm and 148 ppm for the aromatic carbons and a weak signal at 63 ppm assigned to the aliphatic tetragonal carbon that is formed during condensation. The resulting MPN (**P4**) showed maximum S_{BET} values of 1420 $m^2\ g^{-1}$ for homopolymers due to the rigidity and high cross-linking density of the MPNs. Copolymerization of two different monomers followed by supercritical CO_2 treatment ($scCO_2$ washing) led to optimized S_{BET} values up to 1775 $m^2\ g^{-1}$ for a copolymer from monomers **1/3** (1:1 w/w). For comparison, the same, non-$scCO_2$-washed copolymer showed a reduced S_{BET} of 718 $m^2\ g^{-1}$. Therefore, exchange of leftover organic solvents by $scCO_2$ distinctly increases the accessible S_{BET} surface area of the MPNs. This effect was more noticeable for MPNs of lower less cross-linking density in comparison to highly cross-linked MPNs. Optimized homopolymerization of monomer **4** (Scheme 1) with trifluoromethane sulfonic acid as catalyst in 1,2-dichlorobenzene at 140 °C led to MPNs showing high S_{BET} values of up to 2250 $m^2\ g^{-1}$ (Preis et al. 2013). Maximum pore volume and hydrogen storage capacity determined for this MPN (**P4**) are 2.16 $cm^3\ g^{-1}$ and 1.68%, respectively.

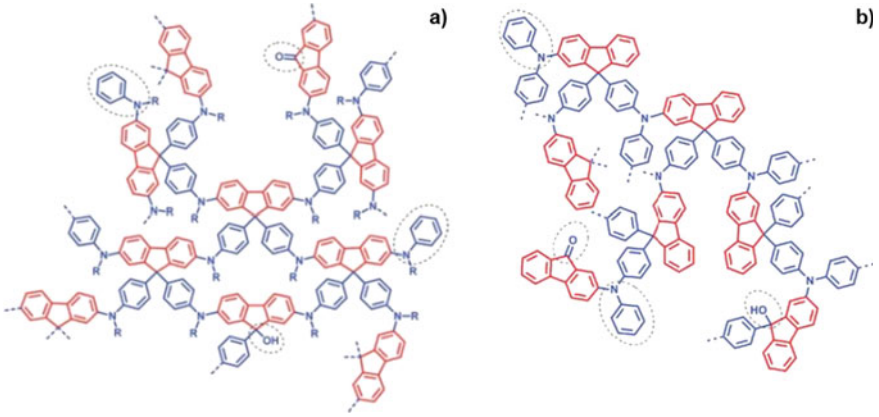

Fig. 2 Idealized chemical structures of MPNs **a** P4 and P5 (P4: R = phenyl and P5: R = methyl), and **b** P6. Unreacted aromatic, keto units and 9-monosubstituted fluorene cores that form end groups cores are encircled. Modified with permission (Preis et al. 2011). Reproduced with permission of The Royal Society of Chemistry

As third example of MPN generation, the metal-free cyclotrimerization of three different aromatic diisocyanate monomers (see monomers **14–16** in Scheme 1) allows for the generation of monolithic MPNs (Preis et al. 2015b). These commercial low-priced monomers undergo cyclotrimerization under triarylcyanurate formation (see Fig. 3a), by using three different catalyst systems: sodium p-toluenesulfinate (p-$TolSO_2Na$), (Moritsugu et al. 2011) tetrabutylammonium fluoride (TBAF) (Nambu and Endo 1993), or tetrakis(dimethylamino)ethylene (TDAE) (Giuglio-Tonolo et al. 2014). A 3 × 7 experimental matrix was set up under variation of monomers, catalysts, solvents, and reaction temperature. Five of the monolithic MPNs obtained from monomer **14** showed a combination of high yield and high S_{BET} surface areas; **P14-1** (92% yield and S_{BET} 783 $m^2\ g^{-1}$: with 10% TBAF in DMI at 150 °C), **P14-2** (92%; 971 $m^2\ g^{-1}$: with 10% TBAF in ODB at 150 °C), **P14-3** (98%; 216 $m^2\ g^{-1}$: with 10% TBAF in THF at 150 °C), **P14-4** (100%; 115 $m^2\ g^{-1}$: with 10% p-$TolSO_2Na$ in DMI at 150 °C), and **P14-5** (86%; 711 $m^2\ g^{-1}$: with 10% TDAE in DMI at room temperature). A second 3 × 15 experimental matrix was applied to optimize the catalyst concentrations (10%, 5% and 1%) for the five promising polymerization conditions. Herein, **P14-6** was obtained under similar condition as **P14-4** with a 1% TBAF resulting in a monolithic MPN with quantitative yield and a S_{BET} value of 1320 $m^2\ g^{-1}$ thus demonstrating the influence of the catalyst/monomer ratio on the cross-linking density of the resulting polymer networks (more than one order of magnitude of improvement in S_{BET}). This easily produced MPN **P14-6** shows reasonably high gas uptakes of 1.3 wt%, 1.1 wt%, and 14.4 wt% for hydrogen (at 77 K), methane (at 273 K), and carbon dioxide (at 273 K), respectively. Moreover, up-scaling the production of **P14-6** was demonstrated by using a 100 g monomer batch resulting in compact, monolithic MPN chunks with a slightly increased S_{BET} of 1510 $m^2\ g^{-1}$. These results suggested potential applications of such MPN monoliths for the capture and storage of gases. It was found that increasing the monomer concentration over a certain threshold leads to the formation of MPNs of higher surface area. This behavior is probably related to an increased cross-linking density.

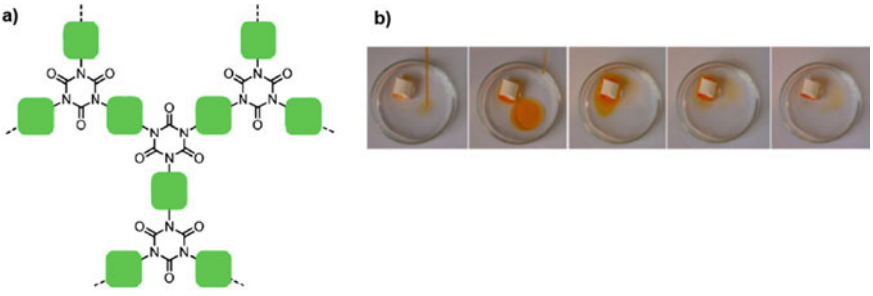

Fig. 3 **a** Idealized chemical structure of the MPNs P14-P16 made from rigid, aromatic diisocyanates (green rectangle represents the aromatic cores: (in P14) 2,2′-dimethyl-biphenyl-1,1′-diyl, (in P15) 1,5-naphthylene and (in P16) 1,4-phenylene, and **b** photographs showing dodecane (dyed with Sudan I) sorption into a microporous, monolithic P14 chunk from aqueous mixture (Preis et al. 2015b). Reproduced with permission of the American Chemical Society

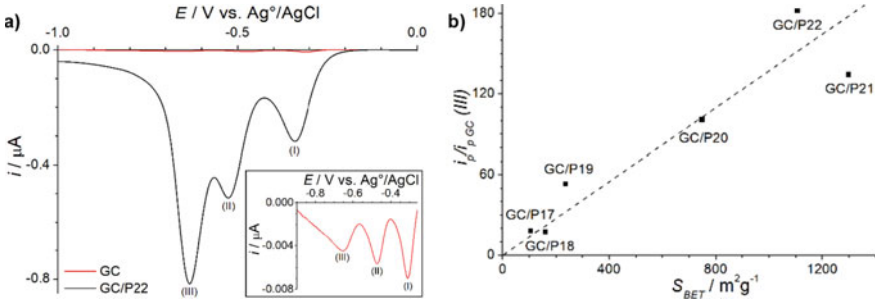

Fig. 4 **a** Linear scan voltammograms (after background correction) for reduction of 0.5 μM aqueous TNB solution at P22-modified and bare (inset) glassy carbon electrodes (at scan rate of 0.01 V s^{-1}) and **b** current ratio of the third reduction peak of TNB at MPN-modified and bare glassy carbon electrodes versus S_{BET} of the MPN films (Palma-Cando and Scherf 2015). Adapted with permission of the American Chemical Society

Removal of oily contaminants from aqueous mixtures was investigated for such **P14** monoliths. Figure 3b shows photographs for the dodecane (as model for an oily contamination, dyed with Sudan I) sorption from an aqueous mixture using microporous **P14** chunks. Hereby, the low-density MPN material (0.18 g cm^{-3}) is floating on the water surface and is completely trapping the oily pollutant (within short times of less than one minute, under up to fourfold mass increase).

3 Electrochemically Synthesized Microporous Polymer Networks

Electrochemical oxidative polymerization of multifunctional monomers with low oxidation potential leads directly to the formation of thin MPN films, while the wet-chemistry based oxidative coupling produces MPN powders (or, in some cases, monoliths) (Palma-Cando and Scherf 2016). Hereby, non-aqueous monomer solutions are usually applied at low concentrations (μM) with supporting organic electrolytes based on tetrabutylammonium salts (Palma-Cando et al. 2014). MPN films can favorably be generated in a three-electrode cell connected to a potentiostat/galvanostat which controls potential and current applied to the system. Microporous polymer films are deposited on the working electrode (WE) by oxidative polymerization. Electronic conductors used as inert WE are usually made of gold, platinum, glassy carbon or ITO (Gurunathan et al. 1999). Our fist approach into the generation of MPN films dealt with the electrochemical polymerization of multifunctional carbazole monomers (for the six investigated monomers see **17–22** in Scheme 1) containing two, three and four carbazole units (Palma-Cando and Scherf 2015). Ambrose and Nelson described the mechanism for the electrochemical oxidative coupling of carbazoles under formation of cation radicals that experience

radicalion-radicalion couplings into 3,3′-bicarbazole dimers (Ambrose and Nelson 1968). Dimers can undergo further reactions such as 6,6′-couplings, into extended oligomers and polymers. In the polymerization of monomers **17–22** we first studied the influence of the number of carbazoles attached to the core of the tectons on the resulting surface area of the deposited microporous polymers. Nitrogen and krypton adsorption isotherms were recorded for the six different MPNs made both by bulk chemical polymerization with $FeCl_3$ (for comparison) and potentiostatic electrochemical polymerization, respectively. Electrogenerated MPN films were synthesized from diluted monomer solutions in acetonitrile/dichloromethane mixtures. Adsorption isotherms of films and powders showed similar trends with a fast N_2 or Kr uptake at low relative pressure (<0.1) which is characteristic for the occurrence of permanent microporosity (Sing et al. 2008). Table 1 lists the S_{BET} values for bulk microporous polymer powders and the respective MPN films. Similar surface area values for bulk polymers and thin films were obtained for the tetrasubstituted MPNs (**P21** and **P22**). On the other hand, decreased S_{BET} values were determined for films generated from bi- and trisubstituted monomers if compared to the corresponding MPN powders (**P17–P20**). Reduced cross-linking density for the electrogenerated films is most probably caused by an exclusive formation of carbazole dimers while $FeCl_3$ bulk polymerization also yields 3,5-disubtituted carbazoles (Chen et al. 2012). Moreover, a direct relationship between the number of carbazole groups in the monomers and the S_{BET} values of the resulting MPN films was observed based on increased cross-linking density and rigidity of the MPNs when increasing the functionality of the monomers. Tetrafunctionalized monomers provide an optimum amount of possible cross-linking sites (Zhang et al. 2014).

Electrogenerated polymer films are very promising materials for the fabrication of electrochemical sensors and biosensors (Terán-Alcocer et al. 2021) for various analytes such as neurotransmitters (Moon et al. 2018), pharmaceuticals (Eslami and Alizadeh 2016), glucose (Naveen et al. 2017), hydrogen peroxide (Park et al. 2016), nitrites (Ge et al. 2020), or nitroaromatic compounds (Guo et al. 2015). We used thin, carbazole-based MPN films for the electrochemical detection of 1,3,5-trinitrobenzene (TNB) as prototypical nitroaromatic compound in aqueous solution, based on its cathodic reduction. An increased current response of up to 182 times was observed for **P22** films on glassy carbon (GC) electrodes when contacted with aqueous TNB solutions, if compared to the current response of bare GC electrodes (see Fig. 4a). An interesting correlation was found between the current response increase (bare GC *vs.* MPN coated GC electrodes) and the S_{BET} of the MPN films (see Fig. 4b). Hereby, the formation of charge-transfer complexes between the electron-poor nitroaromatic analytes and the electron-rich MPN films is boosted by the much higher electroactive surface area at the MPN-modified electrodes where the analyte reduction takes place (Evans et al. 2002; Zhang et al. 2006; Shamsipur et al. 2015).

Regarding civil and environmental security, the detection of explosives in the gas-phase is highly desirable (Sun et al. 2015). Here, fluorescent polymers networks have shown high application potential as luminescent sensor for explosive traces (Liu et al. 2012). We used spirobifluorene-cored MPN films (**P21**) for the gas-phase detection of nitroaromatic explosives due to their intense inherent fluorescence and high S_{BET}

Table 1 Calculated specific BET surface areas S_{BET} of chemically synthesized bulk polymer powders as well as of electrogenerated MPN films using N_2 or Kr gas sorption, respectively

Polymer	Number of electroactive units	S_{BET} powder ($m^2\ g^{-1}$)	S_{BET} film ($m^2\ g^{-1}$)	Polymer	Number of electroactive units	S_{BET} powder ($m^2\ g^{-1}$)	S_{BET} film ($m^2\ g^{-1}$)
P17	2	225	104	P27	4	1322	1106
P18	2	324	159	P28	4	574	492
P19	3	1065	236	P29	8	1331	1027
P20	3	1647	748	P30	8	1194	872
P21	4	1249	1297	P31	4	1097	979
P22	4	1322	1106	P32	4	1039	874
P23	4	1153	815[a] 1240[b]	**P33**	**8**	**2203**	**2170**
P24	4	1102	1099[a] 1576[b]	P34	4	1085	433
P25	4	2020	1258[a] 2135[b]	P35	4	956	–
P26	4	1390	927[a] 1114[b]	P36	8	1767	1634

[a]Solvent: dichloromethane; [b]Solvent: DCM/BFEE

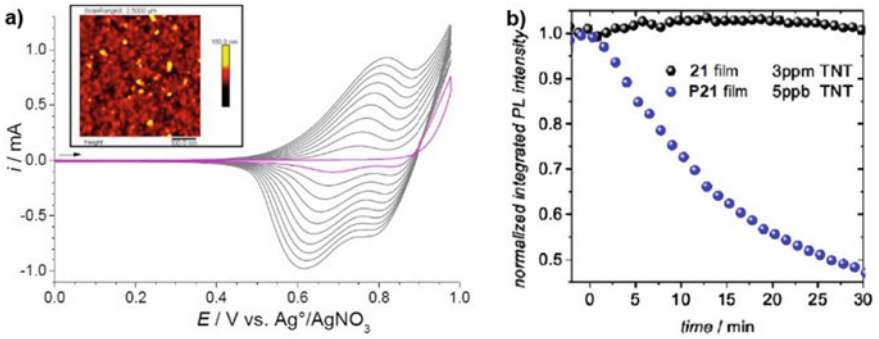

Fig. 5 **a** Ten successive cyclic voltammograms at an ITO electrode for 0.5 mM solution of monomer 21 in acetonitrile/dichloromethane (1:4) and 0.1 M TBAP as supporting electrolyte, potential range: 0–0.98 V, scan rate: 0.10 Vs^{-1}. The inset shows a tapping mode AFM image of the resulting MPN film. **b** Integrated PL response to different TNT vapor concentrations (455–480 nm) for a vapor-deposited non-porous film of monomer 21 (black dots) and a microporous P21-film (blue dots) (Räupke et al. 2016). Reproduced with permission

surface area (1297 m^2 g^{-1}) (Räupke et al. 2016). Figure 5a shows 10 successive voltammetric cycles for the electrochemical polymerization of a 0.5 mM solution of monomer **21** in acetonitrile/dichloromethane (1:4) on ITO electrodes. **P21** thin films with thickness of ca. 50 nm are formed by cycling in a potential range of 0 V–0.98 V with a scan rate of 0.10 Vs^{-1}. A so-called nucleation loop with a crossing effect between the first anodic scan and the reverse sweep is observed during the first cycle. This phenomenon might be related to an autocatalytic reaction between oligomeric intermediates and monomers (Heinze et al. 2007). Tapping mode AFM image shows a rather smooth morphology with a mean roughness Rq of ~14 nm (see inset Fig. 5a). For the sensing experiment, analytes were placed in a closed chamber (analyte chamber) that is connected via a needle valve to a second chamber containing the **P21** films on ITO (sample chamber). Each chamber can be separately heated. Photoluminescence (PL) spectra of a **P21** film upon excitation at 355 nm show a PL peak centered at 472 nm. The so-called quenching efficiency of the **P21** PL upon exposure to different analytes (e.g. acetone, ethanol, toluene, benzene, nitrobenzene—NB, and 2,4-dinitrotolune—DNT) were found to be >1 for electron-poor nitroaromatic analytes (NB and DNT), while for the other analytes only a slight effect on the PL was observed. A possible mechanism of PL quenching is an energy transfer between the excited, electron-rich host and the electron-poor nitroaromatic quencher (Toal and Trogler 2006). The higher quenching efficiency (DNT *vs.* NB) for the energy transfer from the LUMO level of **P21** (−2.58 eV) to the LUMO level of DNT (−3.22 eV) might be ascribed to a deeper lying LUMO level of DNT if compared to the LUMO level position of NB (−2.91 eV). Finally, gas-phase detection of 2,4,6-trinitrotoluene (TNT) at low concentrations down to 5 ppb (room temperature vapor pressure) was investigated. Our **P21** films showed a maximum quenching of ca. 50% after 30 min by contact with TNT vapors (see Fig. 5b). Already after 2–3 min

a significant PL quenching response was recorded. For comparison, PL quenching was not detectable for non-porous films, vapor-deposited films of monomer **21** at even much higher TNT concentration of 3 ppm (3 orders of magnitude increased concentration). These results clearly demonstrate the crucial role of microporosity and high surface area of the films by facilitating the interaction between the MPN surface and the quencher molecules.

In a second attempt, we studied the electrochemical, oxidative polymerization of tetrathienyl-substituted spirobifluorene- and tetraphenylmethane-cored monomers (see monomers **23–26** in Scheme 1) both in pure dichloromethane and dichloromethane/boron trifluoride ethyl etherate (DCM/BFFE) mixtures (Palma-Cando et al. 2015). The coupling mechanism for electron-rich heteroaromatics such as thiophenes is described in a similar way as done for carbazole-based monomers (Diaz et al. 1981). The potential required for the oxidation of the monomer is always higher than potential needed for oxidation of the oligomeric species that are formed in a cascade of condensation reactions toward formation of polymeric chains. It has been demonstrated that the addition of boron trifluoride decreases the needed potential for monomer coupling by reducing the aromaticity of the system through BF_3 interaction with the lone electron pair at the thiophene sulfur (Shi et al. 1995, 1999). The resulting surface areas extracted from nitrogen or krypton sorption measurements of thin, electrogenerated MPN films and, for comparison, of bulk MPN powders obtained by wet-chemical coupling with $FeCl_3$, respectively, are listed in Table 1. The highest S_{BET} surface areas for thin MPN films were achieved for deposition from DCM/BFFE mixtures with S_{BET} values like that of the corresponding bulk polymer powders. This finding indicates the importance of reducing the potential for the monomer oxidation. The connectivity of the networks made from the 3-thienylbased monomers (**24** and **26**) was significantly affected by the presence of boron trifluoride. The formation of hyperbranched oligothiophene structures containing 2,3,5-trisubtituted thiophene units was obtained in electrochemical polymerization in DCM (see Fig. 6a). However, MPN deposition from **24** and **26** in DCM/BFEE mixtures preferably led to the formation of 2,2′-bithiophene links similar to that what is generally observed for the corresponding 2-thienyl-substituted monomers **23** and **25** (see Fig. 6b and c). Moreover, electrochemical reduction of TNB at **P25**-modified GC electrodes showed a linear relationship between current response and thickness of the microporous deposits. These results confirm the role of the donor–acceptor interaction between electron-poor nitroaromatic and electron-rich moieties after modifying GC electrodes with **P25**-films.

In a further study we utilized tetra- and octacarbazole-functionalized monomers with three dimensional, rigid tetraphenylmethane and tetraphenylsilane cores for electrochemical (and wet-chemical) MPN generation (see monomers **27–30** in Scheme 1) (Palma-Cando et al. 2016). Bulk polymer powders were isolated in high yields for the oxidative coupling of these multifunctional monomers with $FeCl_3$. MPN powders showed good thermal stability and intense photoluminescence (PL) with maxima at 444 nm (**P27**), 473 nm (**P28**), 482 nm (**P29**), and 471 nm (**P30**). In addition, a reasonable CO_2 trapping capacity was shown for **P29** with a storage

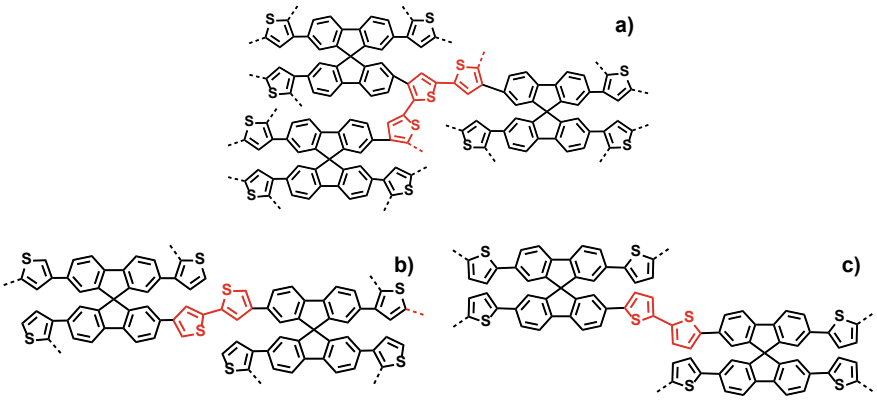

Fig. 6 Idealized chemical structure of the thienyl-thienyl links in microporous films **a** electrochemically prepared P24 in DCM, **b** electrochemically prepared P24 in DCM/BFEE mixture, and **c** wet-chemically prepared P23 (Palma-Cando et al. 2015). Adapted with permission of The American Chemical Society

capacity of up to ca. 9 wt%. Quartz-crystal microbalance measurements simultaneously coupled to the electrochemical film deposition (EQCM) was used for gaining more insight into the growth of the MPN films during the electropolymerization of our multifunctional monomers. The anodic scan in the first cyclic voltammogram for polymerization of monomer **27** showed a decrease in the EQCM frequency starting at the peak potential onset at ca. 0.9 V *vs.* $Ag/AgNO_3$ (see Fig. 7a). These frequency dropping is related to a mass increase that can be estimated by the Sauerbrey equation (Sauerbrey 1959) thus documenting oxidative coupling of carbazole units and subsequent irreversible deposition of a **P27** layer on the Pt/quartz electrode. A continuously increasing mass was observed indicating a homogeneous film growth overlaid by a reversible uptake and release of perchlorate counteranions due to doping/dedoping events in the as-grown **P27** layer. Nitrogen or krypton adsorption isotherms at 77 K for wet-chemically made bulk polymer powders or electrodeposited MPN films are depicted in Fig. 7b and c, respectively. Main gas capture at low relative pressure of <0.1 verifies the microporous nature of the materials. Slightly reduced specific surface areas were found for the electrodeposited MPN films if compared to the bulk polymer powders (see Table 1). **P29** made from octacarbazolyl-substituted tetraphenylmethane tectons showed the highest S_{BET} of 1331 $m^2\ g^{-1}$. Both carbon-cored MPNs displayed increased S_{BET} value in relation to the respective silicon-cored MPNs. This result can be related to electronic $\sigma - \pi$-interactions of aromatic substituents through the silicon centers thus decreasing the reactivity of the carbazolyl groups and leading to a lower cross-linking density (Traylor et al. 1970). Electrochemical sensing experiments for various nitroaromatic analytes were carried out on glassy carbon electrodes modified with microporous **P29** films. Figure 8b depicts linear scan voltammograms for the electrochemical reduction of 0.1 μM solutions

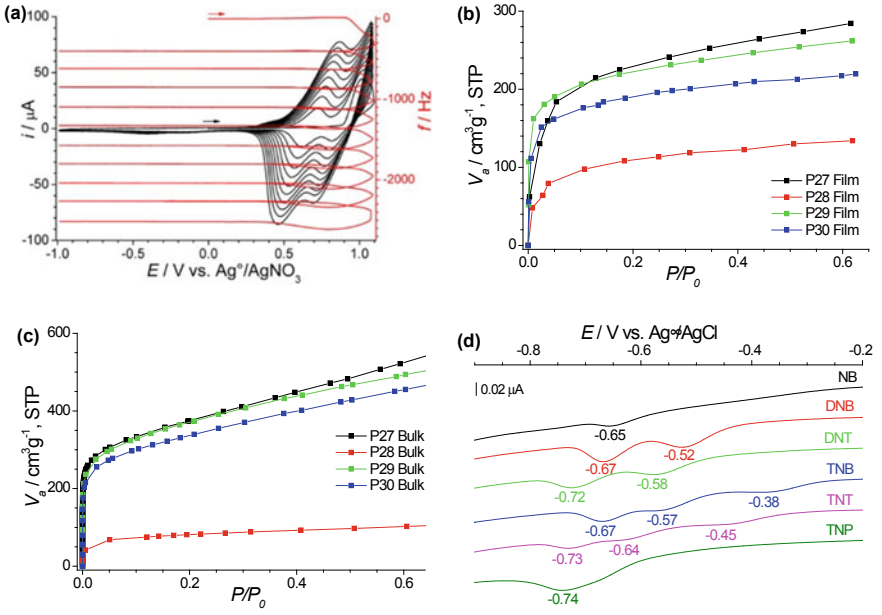

Fig. 7 **a** Ten cyclic voltammograms (black lines) and EQCM frequency changes (red lines), that reflect the mass accumulation in the electrochemical polymerization of 0.1 mM solutions of 27. Adsorption isotherms of **b** electropolymerized MPN films (Kr sorption) and **c** corresponding bulk polymer powders synthesized by oxidative coupling with $FeCl_3$ (N_2 sorption). **d** Linear scan voltammograms for the reduction of 0.1 µM solutions of various nitroaromatic analytes at P29-modified GC electrodes in buffered aqueous solution (pH 7.4). LSVs were obtained with a scan rate of 0.01 V s^{-1} (Palma-Cando et al. 2016). Adapted with permission of the American Chemical Society

of nitrobenzene (NB), 1,3-dinitrobenzene (DNB), 2,4-dinitrotoluene (DNT), 1,3,5-trinitrobenzene (TNB), 2,4,6-trinitrophenol (TNP), and 2,4,6-trinitrotoluene (TNT) at **P29**-modified GC electrodes in an aqueous environment. A series of reduction peaks corresponding to the number of nitro functions in the analyte was observed for sub-µM concentrations of the analytes. Hereby, the position of the first reduction peak potential drops by increasing the number of nitro substituents in the analyte molecules, that means, less energy is required for the initial, interfacial charge transfer between the microporous polymer containing electron-rich bicarbazole-units and the electron-poor nitroaromatic compounds (Shamsipur et al. 2015). Similar results were reported by us for polymer networks deposited from multifunctional monomers with three or six carbazole units (Palma-Cando et al. 2019b).

In a follow-on study, we converted wet-chemically as well as electrochemically a series of six tetra- or octa-substituted carbazole- or thiophene-based, tetraphenylethylene (TPE)-cored monomers (see monomers **31–36** in Scheme 1) into microporous polymer materials (Palma-Cando et al. 2017). TPE is a prominent propeller-shaped structural motif that shows the so-called aggregation-induced emission (AIE)

phenomenon in the solid state. Main reason for occurrence of AIE effects is the restriction of intramolecular rotations and vibrations (Mei et al. 2014). Since early reports of the AIE effect, (Luo et al. 2001; Sharafy and Muszkat 1971) AIE phenomena received enormous attention from the scientific community due to potential applications in different fields (Jimenez and Rodríguez 2020). In our study, luminescent MPN powders based on TPE-cored tectons were obtained by wet-chemical oxidative coupling of monomers **31–36** with $FeCl_3$, resulting in materials that are thermally stable up to 300 °C. Electrochemical, oxidative polymerization of the carbazole-based monomers **31–33** were carried out in dichloromethane solutions containing tetrabutylammonium tetrafluoroborate ($TBABF_4$) as electrolyte, while the thiophene-based monomers **34–36** required the addition of 20% (V/V) BFEE to the solution for effective film formation. Nitrogen or krypton gas adsorption data at 77 K within the relative pressure window of 0–0.6 were determined for bulk polymer powders and MPN films, respectively. A fast gas uptake at low relative pressures documents the microporous nature of the materials. Slightly reduced S_{BET} values were observed for the electrogenerated MPN films if compared to the corresponding bulk powders (see Table 1), probably indicating a reduced cross-linking density. The bulk polymer powders **P31** and **P34** showed quite similar S_{BET} values of ca. 1100 $m^2\ g^{-1}$, both containing tectons that are fourfold carbazolyl- or thienyl-substituted with the substituents directly attached to the TPE core. **P32** and **P35** polymers both containing 1,4-phenylene spacers between the electroactive units and the TPE core showed slightly reduced surface areas of 1039 $m^2\ g^{-1}$ and 956 $m^2\ g^{-1}$, respectively, for the bulk materials/powders. Electrochemically generated **P34** films, as an example for electrodeposited MPN films, display a clearly lowered surface area of only 433 $m^2\ g^{-1}$ possibly related to overoxidation effects due to the high monomer oxidation potential of 1.4 V needed for generation of the thin MPN films and/or to a reduced cross-linking density. By doubling the number of electroactive carbazolyl or thienyl substituents in one monomer, remarkably high S_{BET} values were obtained for **P33** (2203 $m^2\ g^{-1}$) and **P36** polymer powders of (1767 $m^2\ g^{-1}$) indicating high cross-linking density and high rigidity. The presence of the 1,3,5-trisubtituted aromatic spacer units between core fragment and electroactive, peripheral substituents plays, probably, a crucial role concerning the resulting specific surface area: by decreasing the probability for chain intercalation. Within this series, the electrogenerated, carbazole-based MPN films show an intense photoluminescence. The combination of high permanent microporosity and intense PL seems promising for PL sensing applications. Thin MPN films emit green to yellow PL with maxima centered at 527 nm for **P31**, 542 nm for **P32**, and 529 nm for **P33**. Electrogenerated **P33** films were tested as chemical sensors for TNT detection in solution, please note the importance to public health and security (Fei et al. 2014). Figure 8a shows the continuously dropped PL intensity for ppm concentrations of the TNT analyte with a clearly detectable quenching already for a concentration of ~1 ppm TNT. The sensing mechanism can be related to excited state energy transfer between the electron-rich bicarbazole units of the MPN films and the electron-poor

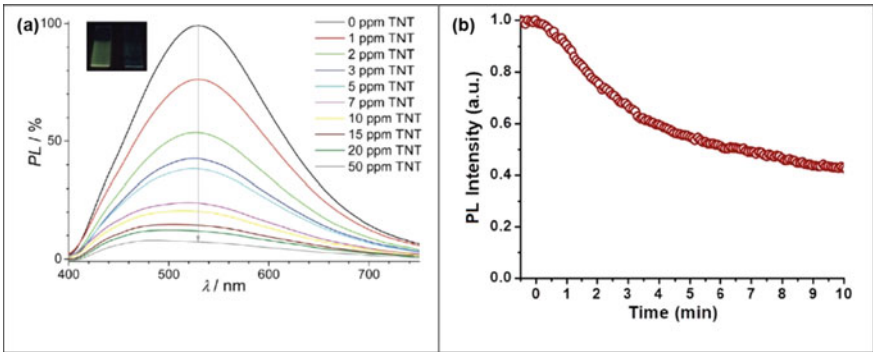

Fig. 8 **a** PL spectra (upon excitation at 340 nm) of P33 films after immersing the films into TNB solutions of different concentrations. The inset shows photographic photoluminescence images of P33 films, in the pristine state and after exposure to 50 ppm TNT solutions. Reproduced with permission (Palma-Cando et al. 2017) Reproduced by permission of The Royal Society of Chemistry. **b** Time trace of the fluorescence quenching of a P31 film in the presence of TNT vapors at a concentration of 10 ppb (Mothika et al. 2018). Reproduced with permission of the American Chemical Society

quencher (TNT). Optimized gas-phase detection conditions for TNT in electrogenerated **P31** films allowed us to detect this harmful analyte up to the 10 ppb level, in a few seconds (see Fig. 8b) (Mothika et al. 2018).

4 Conclusions and Perspectives

During the last decade, our research groups have tested a broad library of new monomers for oxidative generation of microporous polymer networks (MPNs) in wet-chemical and electrochemical strategies. Microporous materials both showing high specific surface areas of up to 2200 $m^2\ g^{-1}$ and intense photoluminescence are accessible by a smart design of the tectons that form the MPN framework (in the case of **P33**, for example, by combining a tetraphenylethylene (TPE) core, phenylene spacers and eight electroactive carbazole units in the periphery). Potential applications in the field of optical or electrochemical sensors for detection of nitroaromatic compounds (including explosives) have been systematically explored, finally allowing for a vapor detection with sensitivities down to a few ppb (e.g. for TNT gas-phase detection). We still see big opportunities in the exploration of related MPNs nanocomposites in fields such as electrochemical sensors, supercapacitors, or heterogeneous catalysis, based e.g. on inherent microporosity, efficient photoluminescence and semiconducting nature of the films. The electrosynthesis of thin MPN films, is, hereby, an elegant and straightforward method to combine MPN synthesis directly with thin film formation.

Acknowledgements A. P.-C. thanks University Yachay Tech for the internal grant No. Chem19-08 and Chem19-17.

References

Ambrose JF, Nelson RF (1968) Anodic oxidation pathways of carbazoles: I . carbazole and N-substituted derivatives. J Electrochem Soc 115:1159–1164. https://jes.ecsdl.org/content/115/11/1159.abstractN2. Electrochemical and spectroscopic techniques have been employed in elucidating the anodic oxidation pathways of carbazole and several N-substituted derivatives. For carbazole and the N-alkyl or N-aryl

Ansems RBM, Scott LT (2000) Circumtrindene: a geodesic dome of molecular dimensions. Rational synthesis of 60 of C 60 1, J Am Chem Soc 122:2719–2724. https://doi.org/10.1021/ja993028n

Bhunia S, Dey N, Pradhan A, Bhattacharya S (2018) A conjugated microporous polymer based visual sensing platform for aminoglycoside antibiotics in water. Chem Commun 54:7495–7498. https://doi.org/10.1039/C8CC02865F

Biswal BP, Becker D, Chandrasekhar N, Seenath JS, Paasch S, Machill S, Hennersdorf F, Brunner E, Weigand JJ, Berger R, Feng X (2018) Exploration of thiazolo[5,4-d]thiazole linkages in conjugated porous organic polymers for chemoselective molecular sieving. Chem A Eur J 24:10868–10875. https://doi.org/10.1002/chem.201802631

Bonillo B, Sprick RS, Cooper AI (2016) Tuning photophysical properties in conjugated microporous polymers by comonomer doping strategies. Chem Mater 28:3469–3480. https://doi.org/10.1021/acs.chemmater.6b01195

Buyukcakir O, Yuksel R, Jiang Y, Lee SH, Seong WK, Chen X, Ruoff RS (2019) Synthesis of porous covalent quinazoline networks (CQNs) and their gas sorption properties. Angew Chemie Int Ed 58:872–876. https://doi.org/10.1002/anie.201813075

Chen L, Honsho Y, Seki S, Jiang D (2010) Light-harvesting conjugated microporous polymers: rapid and highly efficient flow of light energy with a porous polyphenylene framework as antenna. J Am Chem Soc 132:6742–6748. https://doi.org/10.1021/ja100327h

Chen Q, Luo M, Hammershøj P, Zhou D, Han Y, Laursen BW, Yan C-G, Han B-H (2012) Microporous polycarbazole with high specific surface area for gas storage and separation. J Am Chem Soc 134:6084–6087. https://doi.org/10.1021/ja300438w

Dehmlow EV, Kelle T (1997) Synthesis of new truxene derivatives: possible precursors of fullerene partial structures? Synth Commun 27:2021–2031. https://doi.org/10.1080/00397919708006804

Diaz AF, Castillo JI, Logan JA, Lee W-Y (1981) Electrochemistry of conducting polypyrrole films. J Electroanal Chem Interfacial Electrochem 129:115–132. https://dx.doi.org/10.1016/S0022-0728(81)80008-3

Eslami MR, Alizadeh N (2016) Nanostructured conducting molecularly imprinted polypyrrole based quartz crystal microbalance sensor for naproxen determination and its electrochemical impedance study. RSC Adv 6:9387–9395. https://doi.org/10.1039/c5ra21489k

Evans SAG, Elliott JM, Andrews LM, Bartlett PN, Doyle PJ, Denuault G (2002) Detection of hydrogen peroxide at mesoporous platinum microelectrodes. Anal Chem 74:1322–1326. https://doi.org/10.1021/ac011052p

Fei T, Jiang K, Zhang T (2014) Highly sensitive TNT photoluminescent sensing by a phosphorescent complex. Sens. Actuators B Chem 199:148–153. https://dx.doi.org/10.1016/j.snb.2014.03.088.

Ge Y, Jamal R, Zhang R, Zhang W, Yu Z, Yan Y, Liu Y, Abdiryim T (2020) Electrochemical synthesis of multilayered PEDOT/PEDOT-SH/Au nanocomposites for electrochemical sensing of nitrite. Microchim Acta 187:248. https://doi.org/10.1007/s00604-020-4211-1

Geng T-M, Zhu H, Song W, Zhu F, Wang Y (2016) Conjugated microporous polymer-based carbazole derivatives as fluorescence chemosensors for picronitric acid. J Mater Sci 51:4104–4114. https://doi.org/10.1007/s10853-016-9732-y

Giuglio-Tonolo AG, Spitz C, Terme T, Vanelle P (2014) An expeditious method for the selective cyclotrimerization of isocyanates initiated by TDAE. Tetrahedron Lett 55:2700–2702. https://doi.org/10.1016/j.tetlet.2014.03.045

Guo Z, Florea A, Cristea C, Bessueille F, Vocanson F, Goutaland F, Zhang A, Săndulescu R, Lagarde F, Jaffrezic-Renault N (2015) 1,3,5-Trinitrotoluene detection by a molecularly imprinted polymer sensor based on electropolymerization of a microporous-metal-organic framework. Sens Actuators B Chem 207:960–966. https://doi.org/10.1016/j.snb.2014.06.137

Gurunathan K, Murugan AV, Marimuthu R, Mulik UP, Amalnerkar DP (1999) Electrochemically synthesised conducting polymeric materials for applications towards technology in electronics, optoelectronics and energy storage devices. Mater Chem Phys 61:173–191. https://dx.doi.org/10.1016/S0254-0584(99)00081-4

Heinze J, Rasche A, Pagels M, Geschke B (2007) On the origin of the so-called nucleation loop during electropolymerization of conducting polymers. J Phys Chem B 111:989–997. https://doi.org/10.1021/jp066413p

Heinze J, Frontana-Uribe BA, Ludwigs S (2010) Electrochemistry of conducting polymers-persistent models and new concepts. Chem Rev 110:4724–4771. https://doi.org/10.1021/cr900226k

Ibanez JG, Rincón ME, Gutierrez-Granados S, Chahma M, Jaramillo-Quintero OA, Frontana-Uribe BA (2018) Conducting polymers in the fields of energy, environmental remediation, and chemical-chiral sensors. Chem Rev 118:4731–4816. https://doi.org/10.1021/acs.chemrev.7b00482

Jiang J-X, Su F, Trewin A, Wood CD, Campbell NL, Niu H, Dickinson C, Ganin AY, Rosseinsky MJ, Khimyak YZ, Cooper AI (2007) Conjugated microporous poly(aryleneethynylene) networks. Angew Chemie 119:8728–8732. https://doi.org/10.1002/ange.200701595

Jimenez ER, Rodríguez H (2020) Aggregation-induced emission: a review of promising cyano-functionalized AIEgens. J Mater Sci 55:1366–1387. https://doi.org/10.1007/s10853-019-04157-5

Lee J-SM, Cooper AI (2020) Advances in conjugated microporous polymers. Chem Rev 120:2171–2214. https://doi.org/10.1021/acs.chemrev.9b00399

Liao Y, Wang H, Zhu M, Thomas A (2018) Efficient supercapacitor energy storage using conjugated microporous polymer networks synthesized from Buchwald-Hartwig coupling. Adv Mater 30:1705710. https://doi.org/10.1002/adma.201705710

Liu X, Xu Y, Jiang D (2012) Conjugated microporous polymers as molecular sensing devices: microporous architecture enables rapid response and enhances sensitivity in fluorescence-on and fluorescence-off sensing. J Am Chem Soc 134:8738–8741. https://doi.org/10.1021/ja303448r

Liu D-P, Chen Q, Zhao Y-C, Zhang L-M, Qi A-D, Han B-H (2013) Fluorinated porous organic polymers via direct C-H arylation polycondensation. ACS Macro Lett 2:522–526. https://doi.org/10.1021/mz4001699

Lu W, Yuan D, Zhao D, Schilling CI, Plietzsch O, Muller T, Bräse S, Guenther J, Blümel J, Krishna R, Li Z, Zhou H-C (2010) Porous polymer networks: synthesis, porosity, and applications in gas storage/separation. Chem Mater 22:5964–5972. https://doi.org/10.1021/cm1021068

Lu G, Yang H, Zhu Y, Huggins T, Ren ZJ, Liu Z, Zhang W (2015) Synthesis of a conjugated porous Co(II) porphyrinylene–ethynylene framework through alkyne metathesis and its catalytic activity study. J Mater Chem A 3:4954–4959. https://doi.org/10.1039/C4TA06231K

Luo J, Xie Z, Lam JW, Cheng L, Chen H, Qiu C, Kwok HS, Zhan X, Liu Y, Zhu D, Tang BZ (2001) Aggregation-induced emission of 1-methyl-1,2,3,4,5-pentaphenylsilole. Chem Commun 1740–1741. https://doi.org/10.1039/B105159H

Marco AB, Cortizo-Lacalle D, Perez-Miqueo I, Valenti G, Boni A, Plas J, Strutyński K, De Feyter S, Paolucci F, Montes M, Khlobystov AN, Melle-Franco M, Mateo-Alonso A (2017) Twisted aromatic frameworks: readily exfoliable and solution-processable two-dimensional conjugated microporous polymers. Angew Chemie 129:7050–7055. https://doi.org/10.1002/ange.201700271

Mei J, Hong Y, Lam JWY, Qin A, Tang Y, Tang BZ (2014) Aggregation-induced emission: the whole is more brilliant than the parts. Adv Mater 26:5429–5479. https://doi.org/10.1002/adma.201401356

Moon J-M, Thapliyal N, Hussain KK, Goyal RN, Shim Y-B (2018) Conducting polymer-based electrochemical biosensors for neurotransmitters: a review. Biosens Bioelectron 102:540–552. https://doi.org/10.1016/j.bios.2017.11.069

Moritsugu M, Sudo A, Endo T (2011) Development of high-performance networked polymers consisting of isocyanurate structures based on selective cyclotrimerization of isocyanates. J Polym Sci Part A Polym Chem 49:5186–5191. https://doi.org/10.1002/pola.24987

Mothika VS, Räupke A, Brinkmann KO, Riedl T, Brunklaus G, Scherf U (2018) Nanometer-thick conjugated microporous polymer films for selective and sensitive vapor-phase TNT detection. ACS Appl Nano Mater 1:6483–6492. https://doi.org/10.1021/acsanm.8b01779

Nambu Y, Endo T (1993) Synthesis of novel aromatic isocyanurates by the fluoride-catalyzed selective trimerization of isocyanates. J Org Chem 58:1932–1934. https://doi.org/10.1021/jo00059a055

Naveen MH, Gurudatt NG, Shim Y-B (2017) Applications of conducting polymer composites to electrochemical sensors: a review. Appl Mater Today 9:419–433. https://doi.org/10.1016/j.apmt.2017.09.001

Palma-Cando A, Scherf U (2015) Electrogenerated Thin Films of Microporous Polymer Networks with Remarkably Increased Electrochemical Response to Nitroaromatic Analytes. ACS Appl. Mater. Interfaces. 7:11127–11133. https://doi.org/10.1021/acsami.5b02233

Palma-Cando A, Scherf U (2016) Electrochemically generated thin films of microporous polymer networks: synthesis, properties, and applications. Macromol Chem Phys 217:827–841. https://doi.org/10.1002/macp.201500484

Palma-Cando AU, Frontana-Uribe BA, Maldonado JL, Hernández MR (2014) Control of thickness of PEDOT electrodeposits on glass/ITO electrodes from organic solutions and its use as anode in organic solar cells. Procedia Chem 12:92–99. https://doi.org/10.1016/j.proche.2014.12.046

Palma-Cando A, Brunklaus G, Scherf U (2015) Thiophene-based microporous polymer networks via chemical or electrochemical oxidative coupling. Macromolecules. 48. https://doi.org/10.1021/acs.macromol.5b01821

Palma-Cando A, Preis E, Scherf U (2016), Silicon- or carbon-cored multifunctional carbazolyl monomers for the electrochemical generation of microporous polymer films. Macromolecules. 49. https://doi.org/10.1021/acs.macromol.6b02025

Palma-Cando A, Woitassek D, Brunklaus G, Scherf U (2017) Luminescent tetraphenylethene-cored, carbazole- and thiophene-based microporous polymer films for the chemosensing of nitroaromatic analytes. Mater Chem Front 1:1118–1124. https://doi.org/10.1039/C6QM00281A

Palma-Cando A, Rendón-Enríquez I, Tausch M, Scherf U (2019b) Thin functional polymer films by electropolymerization. Nanomaterials 9:1125. https://doi.org/10.3390/nano9081125

Palma-Cando A, Frontana-Uribe BA, Varela-Guerrero V (2019) Relationship between charge transfer diffusion coefficients and doping level for electrogenerated thin PEDOT films on ITO. Bionatura 2. https://doi.org/10.21931/RB/CS/2019.02.01.8

Park CS, Lee C, Kwon OS (2016) Conducting polymer based nanobiosensors, Polymers (Basel) 8. https://doi.org/10.3390/polym8070249

Preis E, Widling C, Scherf U, Patil S, Brunklaus G, Schmidt J, Thomas A (2011) Aromatic, microporous polymer networks with high surface area generated in Friedel–Crafts-type Polycondensations. Polym Chem 2:2186–2189. https://doi.org/10.1039/C1PY00251A

Preis E, Widling C, Brunklaus G, Schmidt J, Thomas A, Scherf U (2013) Microporous polymer networks (MPNs) made in metal-free regimes: systematic optimization of a synthetic protocol toward N-arylcarbazole-based MPNs. ACS Macro Lett 2:380–383. https://doi.org/10.1021/mz400126f

Preis E, Dong W, Brunklaus G, Scherf U (2015a) Microporous, tetraarylethylene-based polymer networks generated in a reductive polyolefination process. J Mater Chem C 3:1582–1587. https://doi.org/10.1039/C4TC02664K

Preis E, Schindler N, Adrian S, Scherf U (2015b) Microporous polymer networks made by cyclotrimerization of commercial, aromatic diisocyanates. ACS Macro Lett 4:1268–1272. https://doi.org/10.1021/acsmacrolett.5b00726

Qiao S, Du Z, Yang R (2014) Design and synthesis of novel carbazole-spacer-carbazole type conjugated microporous networks for gas storage and separation. J Mater Chem A 2:1877–1885. https://doi.org/10.1039/C3TA14017B

Räupke A, Palma-Cando A, Shkura E, Teckhausen P, Polywka A, Görrn P, Scherf U, Riedl T (2016) Highly sensitive gas-phase explosive detection by luminescent microporous polymer networks. Sci Rep 6:29118. https://doi.org/10.1038/srep29118

Sanguinet L, Williams JC, Yang Z, Twieg RJ, Mao G, Singer KD, Wiggers G, Petschek RG (2006) Synthesis and characterization of new truxenones for nonlinear optical applications. Chem Mater 18:4259–4269. https://doi.org/10.1021/cm0601887

Sauerbrey G (1959) Use of quartz vibration for weighing thin films on a microbalance. Zeitschrift Für Phys 155:206–212

Schmidt J, Werner M, Thomas A (2009) Conjugated microporous polymer networks via yamamoto polymerization. Macromolecules 42:4426–4429. https://doi.org/10.1021/ma9005473

Shamsipur M, Tabrizi MA, Mahkam M, Aboudi J (2015) A high sensitive TNT sensor based on electrochemically reduced graphene oxide-poly(amidoamine) modified electrode. Electroanalysis 27:1466–1472. https://doi.org/10.1002/elan.201400634

Sharafy S, Muszkat KA (1971) Viscosity dependence of fluorescence quantum yields. J Am Chem Soc 93:4119–4125. https://doi.org/10.1021/ja00746a004

Shi G, Jin S, Xue G, Li C (1995) A conducting polymer film stronger than aluminium. Science (80-.) 267:994–996. https://doi.org/10.1126/science.267.5200.994

Shi G, Li C, Liang Y (1999) High-strength conducting polymers prepared by electrochemical polymerization in boron trifluoride diethyl etherate solution. Adv Mater 11:1145–1146. https://doi.org/10.1002/(SICI)1521-4095(199909)11:13%3c1145::AID-ADMA1145%3e3.0.CO;2-T

Sing KSW (1985) Reporting physisorption data for gas/solid systems with special reference to the determination of surface area and porosity (recommendations 1984). Pure Appl Chem 57:603–619. https://doi.org/10.1351/pac198254112201

K.S.W. Sing, D.H. Everett, R.A.W. Haul, L. Moscou, R.A. Pierotti, J. Rouquerol, T. Siemieniewska, Reporting Physisorption Data for Gas/Solid Systems, in: Handb. Heterog. Catal., Wiley-VCH Verlag GmbH & Co. KGaA, Weinheim, 2008. https://doi.org/https://doi.org/10.1002/9783527610044.hetcat0065.

Smet M, Schacht E, Dehaen W (2002) Synthesis, characterization, and modification of hyperbranched poly(arylene oxindoles) with a degree of branching of 100%. Angew Chemie Int Ed 41:4547–4550. https://doi.org/10.1002/1521-3773(20021202)41:23%3c4547::AID-ANIE4547%3e3.0.CO;2-A

Sprick RS, Thomas A, Scherf U (2010) Acid catalyzed synthesis of carbonyl-functionalized microporous ladder polymers with high surface area. Polym Chem 1:283–285. https://doi.org/10.1039/B9PY00375D

Sun L, Liang Z, Yu J, Xu R (2013) Luminescent microporous organic polymers containing the 1,3,5-tri(4-ethenylphenyl)benzene unit constructed by Heck coupling reaction. Polym Chem 4:1932. https://doi.org/10.1039/c2py21034g

Sun X, Wang Y, Lei Y (2015) Fluorescence based explosive detection: from mechanisms to sensory materials. Chem Soc Rev 44:8019–8061. https://doi.org/10.1039/C5CS00496A

Suresh VM, Scherf U (2018) Electrochemically generated conjugated microporous polymer network thin films for chemical sensor applications. Macromol Chem Phys 219. https://doi.org/10.1002/macp.201800207

Tan L, Tan B (2017) Hypercrosslinked porous polymer materials: design, synthesis, and applications. Chem Soc Rev 46:3322–3356. https://doi.org/10.1039/C6CS00851H

Terán-Alcocer A, Bravo-Plascencia F, Cevallos-Morillo C, Palma-Cando A (2021) Electrochemical sensors based on conducting polymers for the aqueous detection of biologically relevant molecules. Nanomaterials 11:252. https://doi.org/10.3390/NANO11010252

Toal SJ, Trogler WC (2006) Polymer sensors for nitroaromatic explosives detection. J Mater Chem 16:2871–2883. https://doi.org/10.1039/B517953J

Traylor TG, Hanstein WG, Berwin HJ (1970) σ-π conjugation of carbon-metal bonds. Stereoelectronic and inductive effects. J Am Chem Soc **92**:7476–7477. https://doi.org/10.1021/ja00728a044

Trunk M, Herrmann A, Bildirir H, Yassin A, Schmidt J, Thomas A (2016) Copper-free sonogashira coupling for high-surface-area conjugated microporous poly(aryleneethynylene) networks. Chem A Eur J 22:7179–7183. https://doi.org/10.1002/chem.201600783

Wang X-S, Liu J, Bonefont JM, Yuan D-Q, Thallapally PK, Ma S (2013) A porous covalent porphyrin framework with exceptional uptake capacity of saturated hydrocarbons for oil spill cleanup. Chem Commun 49:1533. https://doi.org/10.1039/c2cc38067f

Wang S, Zhang C, Shu Y, Jiang S, Xia Q, Chen L, Jin S, Hussain I, Cooper AI, Tan B (2017) Layered microporous polymers by solvent knitting method. Sci Adv 3:e1602610. https://doi.org/10.1126/sciadv.1602610

Xie Y, Wang T-T, Liu X-H, Zou K, Deng W-Q (2013) Capture and conversion of CO2 at ambient conditions by a conjugated microporous polymer. Nat Commun 4:1960. https://doi.org/10.1038/ncomms2960

Xu C, Hedin N (2013) Synthesis of microporous organic polymers with high CO2-over-N2 selectivity and CO2 adsorption. J Mater Chem A 1:3406. https://doi.org/10.1039/c3ta01160g

Yuan Y, Zhu G (2019) Porous aromatic frameworks as a platform for multifunctional applications. ACS Cent Sci 5:409–418. https://doi.org/10.1021/acscentsci.9b00047

Zhang H-X, Cao A-M, Hu J-S, Wan L-J, Lee S-T (2006) Electrochemical sensor for detecting ultratrace nitroaromatic compounds using mesoporous SiO2-modified electrode. Anal Chem 78:1967–1971. https://doi.org/10.1021/ac051826s

Zhang K, Kopetzki D, Seeberger PH, Antonietti M, Vilela F (2013) Surface area control and photocatalytic activity of conjugated microporous poly(benzothiadiazole) networks. Angew Chemie Int Ed 52:1432–1436. https://doi.org/10.1002/anie.201207163

Zhang X, Lu J, Zhang J (2014) Porosity enhancement of carbazolic porous organic frameworks using dendritic building blocks for gas storage and separation. Chem Mater 26:4023–4029. https://doi.org/10.1021/cm501717c

Zhang H, Zhang Y, Gu C, Ma Y (2015) Electropolymerized conjugated microporous poly(zinc-porphyrin) films as potential electrode materials in supercapacitors. Adv Energy Mater 5:1402175–1402180. https://doi.org/10.1002/aenm.201402175

Zhang C, He Y, Mu P, Wang X, He Q, Chen Y, Zeng J, Wang F, Xu Y, Jiang J-X (2018) Toward high performance thiophene-containing conjugated microporous polymer anodes for lithium-ion batteries through structure design. Adv Funct Mater 28:1705432. https://doi.org/10.1002/adfm.201705432

Zolotukhin MG, Fomina L, Salcedo R, Sansores LE, Colquhoun HM, Khalilov LM (2004) Superelectrophiles in polymer chemistry a novel, one-pot synthesis of high-T-g, high-temperature polymers. Macromolecules 37:5140–5141. https://doi.org/10.1021/ma0495902